7C.4 CONVECTIVELY FORCED WAVENUMBER-1 VORTEX ROSSBY WAVES IN THE INNER WAVEGUIDE

Israel Gonzalez III* and Hugh E. Willoughby
Florida International University, Miami, Florida

Convectively forced wavenumber-1 Vortex Rossby Waves (VRWs) are intriguing objects for study because, unlike higher wavenumber VRWs, wavenumber 1 forces vortex motion and yields the the widest possible waveguide. A two-dimensional barotropic, nondivergent, vortex-following model is used to simulate VRWs, in a translating cylindrical coordinate system, on an *f*-plane. The forcing approximates Tropical Cyclone (TC) eyewall convection, as a mass source-sink pair that rotates with a specified cyclonic frequency, ω, imposed at the 25-km radius of max (50 ms^{-1}) winds (RMW) in a mean vortex. A Wood-White (2010) profile used to make the axially symmetric vortex is "asymptotically bounded" in a sense that the circulation approaches zero at large radius from the center (Gonzalez *et al*. 2015). Consistent with Stokes' Theorem, the profile exhibits solid rotation in the core, sharp decrease in vorticity with radius, and anticyclonic vorticity in the periphery. The locus of vorticity gradient sign reversal represents the boundary between inner and outer waveguides that support upstream and downstream-propagating waves, respectively. The former is significant for this study.

Specified frequencies of the forcing are initialized as different fractions of the mean-flow angular velocity at the RMW ($\omega_o=2x10^{-3}s^{-1}$), that range between $0.25\omega_o$ and ω_o. The model reads the vortex properties from a setup file, calculates vorticity, marches vorticity forward in time in 150-s time steps, inverts vorticity to solve for the streamfunction using a Lindzen-Kuo (1969) Poisson solver, and tracks the moving vortex's center for 24 simulated hours. A pair of rotating gyres with opposing polarity form near the core and have maximum amplitudes at the forcing locus as the vortex axisymmetrizes with time (Figure 1). Excited VRWs propagate upon the mean vortex's negative radial vorticity gradient within an inner waveguide (*Cotto et al. 2015*) confined between an inner turning point and outer critical radius. The former is associated with the one-dimensional VRW (Ω_{1D}), cutoff frequency – the greatest (most negative)

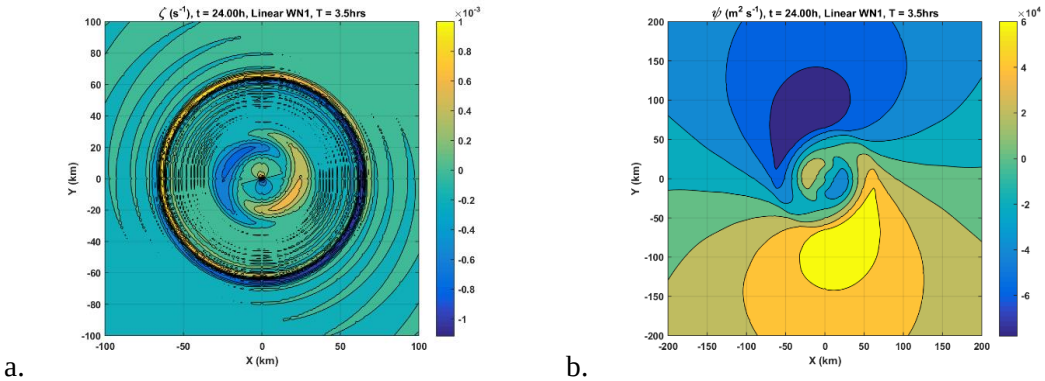

a. b.

Figure 1. Filled contour plots for perturbation vorticity (a) and streamfunction (b), illustrating wavenumber-1 gyres arising from the forcing with an orbital period of 3.5 hrs (~6.9 rotations per 24-hr simulation). Since vorticity is inverted in the Poisson solver, positive streamfunction (warm colors) corresponds to anticyclonic flow.

* Corresponding Author Address: Israel Gonzalez III, Dept. of Earth and Environment, Florida International University, Miami, FL 33199. Email: igonz008@fiu.edu
Phone: 305-348-1930. Room: AHC5-356.

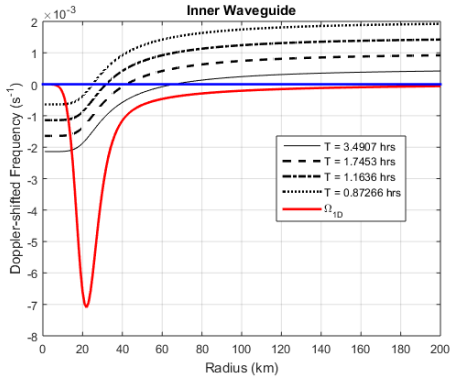

Figure 2. Wavenumber-1 VRW inner waveguide highlighting the frequency passbands for different ranges of orbital periods (T = 2π/ω).

frequency a VRW can assume. Therefore, the inner waveguide (Figure 2) can support only a select range of VRWs propagating with negative Doppler-shifted frequencies: $\Omega = \omega - V_o/r$. The last term is the mean-flow angular velocity at a given radius.

The waves propagate away from the forcing locus with an upstream phase velocity and downstream group velocity, relative to the mean swirling flow. Initially inward propagating VRWs are Doppler-shifted to Ω_{1D}, become radially long, reflect from a turning point a few kilometers inward from the RMW, and then move outward to the critical radius where wave energy is ultimately absorbed and transferred to the mean flow. An outward geopotential flux from the RMW that convergences near the critical radius occurs as a result. These VRWs also converge angular momentum into the forcing locus at the RMW, thus accelerating the mean flow and intensifying the vortex. Though, deceleration of similar magnitude occurs in the neighborhood of the critical radius, where there is strong angular momentum flux divergence.

The critical radius is where the group velocity and Ω of radially short, outward-propagating VRWs approaches zero (i.e., $\omega \rightarrow V_o/r$), causing vorticity and wave energy to accumulate at the waveguide's outer boundary to become tightly wound, filamented trailing spirals that wrap around the vortex core to resemble observed TC rainbands on radar (Figure 1a). The diameter of the symmetric, interlocked vorticity spirals shrinks as ω increases. Numerous vorticity filaments appear between the forced gyres and critical radius, indicating outward VRW propagation. Beyond the critical radius is the evanescent region where some wave energy leaks outward and decays exponentially. Waves in the evanescent region have a positive Ω (i.e., $\omega > V_o/r$). A vorticity "wake" also seen ahead and behind the translating vortex, aligns with the slipstream flow and vortex's direction of motion.

Vortex motion arises from the counterflow between the inner streamfunction gyres (Figure 1b) that advects vorticity across the vortex center, analogous with the beta gyres in the outer waveguide. Translation through the quiescent environment causes a slipstream flow that feeds angular momentum and anticyclonic vorticity into the vortex core. The slipstream also interacts with the vortex's mean swirling flow to form an outer streamfunction dipole of large, cyclonically curved gyres that essentially rotates with the wind, around smaller, convectively forced inner gyres. The locus where the teardrop-shaped, cyclonic (anticyclonic) outer gyre curves into the inner gyres, aligns with the vortex's direction of motion (slipstream). A smooth, counterclockwise track at low speeds with

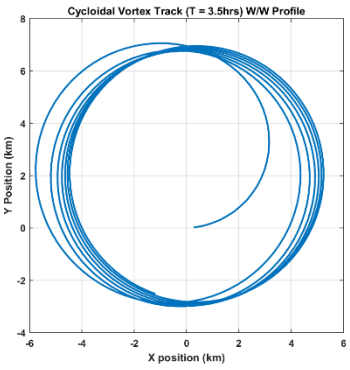

a.

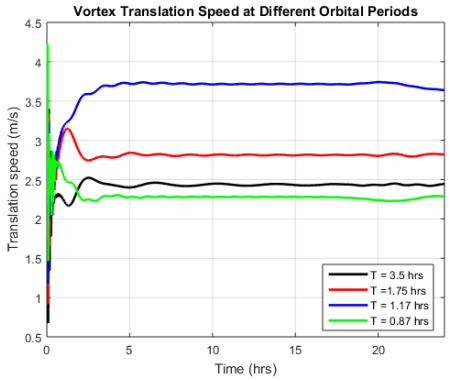

b.

Figure 3. Vortex trochoidal track for a 3.5-hr orbital period (a) and translation speed at different orbital periods (b). Generally, the greater the orbital period, the larger the track diameter and the slower the translation speed.

frequency ω ensues, plausibly simulating trochoidal motion (Nolan *et al*. 2001) observed in real TCs (Figure 3). Translation speed and orbital track diameter are modulated by ω – low values slightly decrease speed but the orbital track diameter increases. The former is more sensitive to changes in ω. Frequency passband width is also determined by ω. The widest passbands, with critical radii ranging between ~60 and ≥100km from the vortex center, coincides with low frequencies, therefore increasing the distance of wave transport. In summary, the faster the forcing rotates, the larger (smaller) the vortex translation speed (track orbital diameter). Frequency passband width also decreases.

It is important to note that the threshold to support VRW propagation without incurring radial wave trapping between two turning points is ~ $0.08\omega_o$. The forcing of trapped waves must rotate very slowly, or anticyclonically, against the swirling wind. Either scenario results in continuous wave reflection within a very narrow radial interval that excludes the critical radius. If ω is negative, then the vortex acquires a clockwise track, showcasing the vortex's proclivity to follow the rotating vorticity source-sink pair. Although it was initially hypothesized that the indefinite wave reflection would build up energy to high amplitudes to intensify the vortex, trapped waves instead demonstrated that unimpeded wave propagation appears important for spiral band formation.

The results from Cotto *et al*. (2015) show that wavenumber ≥ 2 VRWs are illustrated as a wavetrain of eddies with alternating polarity that get advected downstream by the vortex's mean swirling flow. This configuration produces a deformational flow in the vortex core that precludes vorticity-advection-induced storm motion. Instead, a balanced vorticity exchange between the eye and eyewall occurs; one plausible mechanism for eyewall mesovortices (Kossin and Schubert 2001). Since only wavenumber 1 produces two gyres rotating around each other, vorticity is not exchanged but rather, gets persistently advected across the vortex center in different directions which produces the trochoidal track discussed earlier. Despite notable differences between wavenumber 1 and wavenumbers ≥ 2, essential VRW dynamics are captured from both perspectives. Wavenumbers 1 and 2 are most significant because their wide waveguides increase flexibility of wave transport, and range of propagation frequencies. Furthermore, cyclonically curved, low-wavenumber spirals have been observed within the cores of real TCs (e.g., Reasor *et al*. 2000).

References

Cotto, A., I. Gonzalez III, and H.E. Willoughby, 2015: Synthesis of Vortex Rossby Waves. Part I: Vortex Episodically Forced Waves in the Inner Waveguide. *J. Atmos Sci*., **72**, 3940-3956.

Gonzalez, I., III, H.E. Willoughby, and A. Cotto, 2015: Synthesis of Vortex Rossby Waves. Part II: Vortex Motion and Waves in the Outer Waveguide. *J. Atmos Sci*., **72**, 3958-3974.

Kossin, J.P., and W.H. Schubert, 2001: Mesovortices, Polygonal Flow Patterns, and Rapid Pressure Falls in Hurricane-Like Vortices. *J. Atmos Sci*., **58**, 2196-2209.

Lindzen, R.S., and H.L. Kuo, 1969: A Reliable Method for the Numerical Integration of a Large Class of Ordinary and Partial Differential Equations. *Mon Wea Rev*., **97**, 732-734.

Nolan, D.S., M.T. Montgomery, and L.D. Grasso, 2001: The Wavenumber-One Instability and Trochoidal Motion of Hurricane-like Vortices. *J. Atmos. Sci*., **58**, 3243-3270.

Reasor, P. D., M. T. Montgomery, F. D. Marks Jr., and J. F. Gamache, 2000: Low-wavenumber structure and evolution of the hurricane inner core observed by airborne dual-Doppler radar. *Mon. Wea. Rev*., **128**, 1653–1680.

Wood, V.T., and L.W. White, 2010: A New Parametric Model of Vortex Tangential-Wind Profiles: Development, Testing, and Verification. *J. Atmos Sci*., **68**, 990-1006.